11-7-2018

Evidence for a Partially Stalled γ Rotor in F

Angela Murcia Rios

Siavash Vahidi

Stanley D Dunn

Lars Konermann

Evidence for a Partially Stalled γ Rotor in F_1-ATPase from H/D Exchange Experiments and Molecular Dynamics Simulations

Angela Murcia Rios[1], Siavash Vahidi[1], Stanley D. Dunn*, and Lars Konermann*

Departments of Chemistry and Biochemistry, The University of Western Ontario, London, Ontario, N6A 5B7, Canada

* To whom correspondence should be addressed. E-mail: konerman@uwo.ca or sdunn@uwo.ca.

[1] These two authors contributed equally.

Funding was provided by the Natural Sciences and Engineering Research Council of Canada (RGPIN-2018-04243 to L.K.), and the Canadian Institutes of Health Research (FRN 10237, S.D.D.).

Abstract: F_1-ATPase uses ATP hydrolysis to drive rotation of the γ subunit. The γ C-terminal helix constitutes the rotor tip that is seated in an apical bearing formed by $\alpha_3\beta_3$. It remains uncertain to what extent the γ conformation during rotation differs from that seen in rigid crystal structures. Existing models assume that the entire γ subunit participates in every rotation. Here we interrogated *E. coli* F_1-ATPase by H/D exchange (HDX) mass spectrometry. Rotation of γ caused greatly enhanced deuteration in the γ C-terminal helix. The HDX kinetics implied that most F_1 complexes operate with an intact rotor at any given time, but that the rotor tip is prone to occasional unfolding. A molecular dynamics (MD) strategy was developed to model the off-axis forces acting on γ. MD runs showed stalling of the rotor tip and unfolding of the γ C-terminal helix. MD-predicted H-bond opening events coincided with experimental HDX patterns. Our data suggest that *in vitro* operation of F_1-ATPase is associated with significant rotational resistance in the apical bearing. These conditions cause the γ C-terminal helix to get "stuck" (and unfold) sporadically while the remainder of γ continues to rotate. This scenario contrasts the traditional "greasy bearing" model that envisions smooth rotation of the γ C-terminal helix. The fragility of the apical rotor tip in F_1-ATPase is attributed to the absence of a c_{10} ring that stabilizes the rotation axis in intact F_oF_1. Overall, the MD/HDX strategy introduced here appears well suited for interrogating the inner workings of molecular motors.

Introduction

F_oF_1 is a membrane-bound molecular motor that is capable of using protonmotive force (PMF) to synthesize adenosine triphosphate (ATP) from adenosine diphosphate (ADP) and inorganic phosphate.[1-4] The *E. coli* system has the subunit composition $\alpha_3\beta_3\gamma\delta\varepsilon ab_2c_{10}$, where $\gamma\varepsilon c_{10}$ represents the central rotor. The membrane-embedded c_{10} ring forms the basal rotor end. At the opposite (apical) end of the rotor, the γ C-terminal helix reaches into the catalytic head where $\alpha_3\beta_3$ forms an apical bearing. (Figure 1a).[1,2,5-12] Under ATP hydrolysis conditions the rotation of $\gamma\varepsilon c_{10}$ is driven by movements of the β-levers that apply off-axis forces to γ.[12,13] Each β catalytic site successively switches through three states ($\beta_{ATP} \rightarrow \beta_{ADP} \rightarrow \beta_{empty} \rightarrow ...$),[14] and each of these transitions advances $\gamma\varepsilon c_{10}$ by 120°.[2,15-17] Rotation of c_{10} causes vectorial proton transport.[9,12,18,19]

Experiments and molecular dynamics (MD) simulations have uncovered many of the principles underlying F_oF_1 operation.[1,2,5-13,16,20,21] Nonetheless, the exact conformational transitions of individual subunits during rotational catalysis remain incompletely understood. These knowledge gaps arise from the fact that static crystallographic and cryo-EM data do not reveal all of the mechanistically important movements. Spectroscopic tools can provide insights into such dynamic features, but the structural resolution of those experiments tends to be limited.[5,6,16,22-27]

Hydrogen deuterium exchange (HDX) mass spectrometry (MS) can probe dynamic motions of proteins.[28-36] Backbone amide deuteration in folded regions is mediated by H-bond opening/closing fluctuations.[37,38] At pH 8 (which is commonly used for F_oF_1 studies[39,40]) the intrinsic exchange of unprotected amides occurs with $k_{int} \approx 10$ s^{-1} at room temperature.[41] Protein dynamics associated with closing events much faster than k_{int} give rise to EX2 conditions, where isotope envelopes gradually shift to higher mass. Conversely, the EX1 regime is characterized by

closing rates much slower than k_{int}. Such EX1 dynamics usually take place in the form of cooperative (collective) fluctuations that give rise to bimodal isotope envelopes.[32,42-44]

We recently applied HDX-MS to F_oF_1.[40] The γ C-terminal helix exhibited elevated deuteration during ATP hydrolysis-driven rotation. We attributed this effect to torsional stress arising from rotor over-twisting, mediated by the interplay of β-lever action and friction-like γ···$\alpha_3\beta_3$ contacts in the apical bearing. This destabilization of γ was observed only during operation against a PMF-induced torque; the effect disappeared when PMF was eliminated by an uncoupler. We noted[40] that this behavior is analogous to that of macroscopic powertrains, where bearings inflict greater forces on the drive shaft when a motor is under load than during idling.[45] However, the role of friction-related phenomena in molecular motors remains controversial,[20,24,46] and the understanding of such effects in F_oF_1 is rudimentary.[40]

Unravelling the inner workings of F_oF_1 is complicated by its many interacting subunits and PMF-energized membrane. F_1-ATPase is a water soluble F_oF_1 subcomplex. It represents a more tractable system that retains the ability to drive γ rotation via ATP hydrolysis.[16,23-27,47] F_1-ATPase from *E. coli* has the composition $\alpha_3\beta_3\gamma\delta\varepsilon$[14,17,21,48-50] (MW 382 kDa, Figure 1b).[5,27] Due to the lack of a c_{10} ring, the "foot" of γ protrudes into the solvent. Because of its reduced size F_1-ATPase is well suited for exploring the conformational dynamics of the γ rotor, and the role of γ···$\alpha_3\beta_3$ contacts in the apical bearing. It has traditionally been envisioned that hydrophobic residues lining the inside of the apical bearing allow smooth rotation of the γ C-terminal helix (together with the rest of γ).[14] Interestingly, Hilbers et al.[51] recently demonstrated that γ rotation in F_1-ATPase still takes place after disulfide linking the γ C-terminal helix with $\alpha_3\beta_3$. Thus, F_1-ATPase can function with a stalled ("stuck") apical rotor tip, via local unfolding of the γ C-terminal helix with swivel rotation around ϕ/Ψ angles.[51] The implications of those findings[51] for unmodified F_1-ATPase are

unclear. It remains to be established if all parts of γ participate in rotation under normal operating conditions.

In the present study we conducted the first HDX-MS investigation of F_1-ATPase. Our work employed working/inhibited state comparisons. To distinguish trivial substrate binding effects from features that are uniquely linked to rotation we examined three non-rotating states. (i) The ADP-inhibited state I_{ADP} has Mg·ADP and azide permanently bound in at least one catalytic site.[25,52] (ii) $I_{AMP\text{-}PNP}$ represents a state where the enzyme binds azide and the non-hydrolyzable substrate analog AMP-PNP.[52] (iii) The Mg^{2+}-depleted state $I_{Mg\text{-}dep}$ represents F_1-ATPase that is essentially nucleotide-free because its nucleotide binding affinity is reduced by orders of magnitude.[53] (iv) In addition to these three inactive states we characterized the working state *W* where F_1-ATPase underwent ATP hydrolysis-driven γ rotation.

The HDX-MS experiments of this work were complemented by all-atom steered MD simulations[54-56] designed to mimic the off-axis forces acting on γ during rotation. HDX-MS revealed significant destabilization of H-bonds in the γ C-terminal helix during rotational catalysis. MD simulations uncovered that this effect arises from occasional stalling of the over-twisted helix in the apical bearing. Our data imply that movement of γ within the apical bearing is associated with significant rotational resistance, very different from the previously envisioned "hydrophobically greased"[14,57] rotation. The current work marks the first time that a combined MD/HDX approach was applied to a motor protein. The findings obtained have general implications for the behavior of rotor/bearing systems in molecular machines.

Methods

Materials. Tricine, adenosine 5′-diphosphate (ADP) sodium salt, adenosine 5'-triphosphate disodium trihydrate salt (ATP), adenosine 5′-(β,γ-imido)triphosphate lithium salt hydrate (AMP-PNP), mono-cyclohexylammonium phosphoenolpyruvic acid (PEP, adjusted to pH 7), (ethylenedinitrilo)tetraacetic acid (EDTA), NaN_3, $MgCl_2$, NaI, KCl, and rabbit muscle pyruvate kinase were obtained from Sigma (St. Louis, MO, USA). Formic acid, acetonitrile, and water were of LC-MS grade and came from Fisher Scientific (Nepean, Ontario, Canada). D_2O was from Cambridge Isotope Laboratories (Andover, MA). Wild-type *E. coli* F_1-ATPase was prepared from strain AN1460[58] carrying plasmid pAN45 that directs moderate constitutive overexpression of ATP synthase, as described previously[59] except that the size exclusion chromatography step was carried out using a Sephacryl S-400 HR column.

HDX Sample Preparation. Samples for HDX-MS contained 50 mM tricine buffer, 50 mM KCl, and 60 mM PEP at $pH_{corrected}$ 8.[60] Each experiment included an initial equilibration step during which the condition of interest (I_{ADP}, $I_{AMP\text{-}PNP}$, $I_{Mg\text{-}dep}$, W, as defined in the Introduction) was imposed via a two-fold dilution of F_1 stock solutions into H_2O-based buffer. The equilibration time was 60 min for inhibited samples, and 1 min for W. The four sample types differed in the following aspects: The working state W was implemented by employing a pyruvate kinase/PEP ATP-regenerating system (0.1 mg mL^{-1} pyruvate kinase, 0.5 mM ATP, and 4 mM $MgCl_2$) that maintained a high ATP:ADP ratio and ensured catalytic turnover without ADP inhibition.[25] Following established protocols[52] I_{ADP} and $I_{AMP\text{-}PNP}$ samples were supplemented with 0.1 mM ADP, 4 mM $MgCl_2$, and 3 mM NaN_3. In addition, the I_{ADP} contained 0.5 mM ATP, while $I_{AMP\text{-}PNP}$ contained 0.5 mM AMP-PNP. Lastly, $I_{Mg\text{-}depleted}$ was implemented by addition of 1 mM EDTA.[53] HDX was initiated by tenfold dilution into a D_2O-based labeling buffer that contained additives

identical to those of the equilibrated mixtures, for a final F_1-ATPase concentration of 0.125 μM. Deuteration was conducted at 22 ± 1 °C with labeling times between 10 s and 45 min, as this was the approximate interval during which *W* could sustain rotational catalysis under the conditions used here. The activity of *W* under HDX conditions was k_{cat} = 17 s^{-1}, corresponding to ~15000 complete γ rotations during the 45 min experimental window. HDX was quenched by acidification of the solutions to pH_{read} 2.4 using 10% (v/v) formic acid and immediately flash frozen in liquid N_2. Unlike F_oF_1 membrane vesicles,[40] isolated F_1 did not aggregate upon acidification.

Mass Spectrometry. The workflow of our peptide-level resolved HDX-MS experiments was similar to that described previously,[40] using a HDX nanoAcquity UPLC and a Waters Synapt G2 mass spectrometer (Waters, Milford, MA, USA) operated in ion mobility mode at an electrospray voltage of +3 kV. The RF-only quadrupole was set to dwell at *m/z* 300 to prevent low mass contaminants from interfering with analytically valuable peptides. The mass spectrometer was initially calibrated externally using NaI, followed by dynamic lock spray calibration using leucine enkephalin. Identification of peptic peptides was performed by drift time-aligned MS^E with PLGS 2.5.3 (Waters) analysis by searching against the entire *E. coli* proteome plus porcine pepsin. Sequence coverages were 90% for both α and β, 83% (γ), 70% (δ), and 63% (ε) (Figure S1). For HDX measurements 150 μL of quenched HDX samples, containing ~2.5 μM of F_1, were thawed on ice and loaded onto the 50 μL UPLC injection loop. Online digestion was performed using a POROS pepsin column (2.1 mm × 30 mm, Applied Biosystems, Carlsbad, CA) at 15 °C. Peptides were trapped on a BEH130 C18 (2.1 mm × 5 mm) VanGuard column at 100 μL min^{-1} for 2 min. Separation was achieved on a BEH130 C8 (2.1 mm × 50 mm) column at 0 °C at a flow rate of 100 μL min^{-1} with a 15 minute water/acetonitrile gradient acidified using 0.1% formic acid. Extensive

cleaning and blank injections in-between sample runs ensured the absence of carryover. HDX data analyses were performed using DynamX 3.0 (Waters). The level of deuterium uptake at time t is reported as % D (t) = ($m_t - m_0$)/ ($m_{100} - m_0$) where m_t is the centroid m/z for the peptide of interest at time t. m_0 and m_{100} correspond to minimally and fully deuterated controls, respectively. The m_0 samples were prepared by adding isolated F_1 to a pre-quenched solution with a composition identical to that of the I_{Mg_dep} samples, followed immediately by flash freezing. m_{100} samples were prepared similar to m_0 samples, except that they were incubated for ~ 5 days at room temperature prior to flash freezing. Back-exchange levels were (31 ± 8)%, consistent with literature data.[61] The %D normalization strategy used here with proper m_0 and m_{100} controls corrects for this unavoidable back-exchange as well as in-exchange.[62] All %D values are averages of three independent replicates; error bars in uptake plots represent standard deviations. Residue numbering for all HDX experiments corresponds to the *E. coli* X-ray structure 3OAA.[13]

Molecular Dynamics Simulations. All-atom MD runs were conducted using Gromacs 2016.4 with GPU acceleration,[63] the CHARMM36 force field, [64] and TIP3P water.[65] Most simulations were conducted on the *E. coli* $\alpha_3\beta_3\gamma$ complex (3OAA, structure #1).[13] Mg·AMP-PNP in the three noncatalytic α-sites was modified to Mg·ATP.[13] In 3OAA the β_{TP} and β_E sites are empty, while the β_{DP} site is occupied by Mg·ADP. Unless noted otherwise, simulations were conducted with nucleotides bound only to the noncatalytic sites. Additional runs were conducted with one or two nucleotides bound to the catalytic sites. Missing residues and side chains were inserted using PyMOL. The extended N-terminal tails of α (α1-26) were truncated to reduce the size of the simulation box. To avoid rotation of the entire complex and to mimic the immobilization technique used in some experiments[16,23-27,47] the N-terminal crown of the three β-subunits (β9-80)

was restrained[17,56] using a force constant of 1000 kJ mol^{-1} nm^{-2}. All run conditions were initially tested and validated using bovine $\alpha_3\beta_3\gamma$ F_1-ATPase (1E79)[66] which had been used for previous simulations.[17,21,67] For implementing periodic boundary conditions F_1-ATPase was centered in a box with a minimum distance of 1 nm from the edges. Titratable sites were set to their canonical charge states. The Verlet cut-off scheme was used for neighbor search with 1 nm electrostatic and van der Waals cut-offs, and with particle mesh Ewald summation for long-range electrostatics.[68] 150 mM NaCl was added and additional ions were included to make the system neutral. After steepest descent energy minimizations the system was NVT and NPT equilibrated (1 bar, 310 K, 100 ps each) using a velocity-rescaling thermostat[69] and Parrinello-Rahman barostat.[70] Initial velocities were sampled from a Maxwell-Boltzmann distribution. NPT production runs were performed starting from the equilibrated system with the Nosé-Hoover[71] thermostat at 310 K and 1 bar with a 2 fs time step. Bonds were constrained using the linear constraint solver algorithm.[72]

Steered MD was applied to drive rotation of γ by 120°. Two different protocols were applied: (1) *Enforced bulk rotation* was conducted in a rhombic dodecahedral box (~313,000 atoms) using the flex2-t flexible axis method of Grubmüller (Figure 2a).[73,74] Within this approach γ was divided into 1.5 nm thick slabs that were perpendicular to the rotation vector defined by the longest principal axis of the $\alpha_3\beta_3$ stator. A rotation potential with a force constant of 400 kJ mol^{-1} nm^{-2} and a rotation rate of 21° ns^{-1} was applied to all atoms in each slab. Hence, all of γ served as rotation group,[73,74] and each γ residue was forced to move on a circular trajectory.

(2) For this work we also developed an *off-axis force* algorithm that employed center-of-mass (COM) pulling[55] in a cubic box (~787,000 atoms). To mimic a β-lever-mediated power stroke, residues γ20-26[17,71] were subjected to a pulling force (Figure 2b).[17,56] This was achieved by applying a harmonic potential with a force constant of 1000 kJ mol^{-1} nm^{-2} to the γ20-26 COM.

Pulling speeds along a directional vector **D** were between 2.2 nm ns^{-1} and 0.15 nm ns^{-1}. Proper movement of γ20-26 was achieved by updating **D** in 10 ps intervals. The three C_α atoms of residues β11 (β19 for bovine F_1) represented the reference group. The normal vector at the center of the plane defined by the reference group served as rotation axis. In this way, the COM of γ20-26 was forced to move around this axis on a circular trajectory along pre-defined points (see Figure S2 for details). The trajectory radius was (1.4 ± 0.1) nm, where the ± variation reflects the slightly different locations of the γ20-26 COM after equilibration. For smooth trajectories the specified pulling speeds would provide rotation rates between 91° ns^{-1} and 5.6° ns^{-1}. However, directional fluctuations increased the time required to complete the runs. Actual rotation rates were between 29° ns^{-1} and 3.3° ns^{-1}. These conditions are well within the range of γ rotation rates used for previous simulations which include 120° ns^{-1},[56] 20° ns^{-1},[17,73] 1-10° ns^{-1},[20] 3° ns^{-1},[67] and 0.42° ns^{-1}.[74] No restraints were applied to γ during off-axis force simulations.

Results and Discussion

Selected Peptide Mass Spectra. For exploring the F_1-ATPase conformational dynamics we performed HDX-MS experiments on the working state *W* which undergoes ATP-driven γ rotation. Control experiments were performed on the inactive forms I_{ADP}, $I_{AMP\text{-}PNP}$, and $I_{Mg\text{-}dep}$. Figure 3 exemplifies unprocessed data for selected peptides, focusing on a deuteration time of t = 45 min.

Pronounced differences between I_{ADP}, $I_{Mg\text{-}dep}$, and *W* were observed in the catalytic sites. Spectra for the P-loop are displayed in the first column of Figure 3 (peptide β148-159). The P-loop is in contact with the ATP/ADP phosphate groups.[14] Gaussian decomposition of the P-loop spectra for I_{ADP} and $I_{Mg\text{-}dep}$ suggests three distinct components, consistent with three conformations β_{ATP},

β_{ADP}, and β_{empty}. We tentatively assign the most heavily deuterated component to β_{empty}, which has several disrupted H-bonds between strands 3/7.[14] Under *W* conditions the P-loop HDX spectrum coalesced into a single band, reflecting conformational averaging caused by the $\beta_{ATP} \rightarrow \beta_{ADP} \rightarrow \beta_{empty} \rightarrow$ ... interconversion during ATP-driven γ rotation.[40]

The catalytic site peptide β241-249 exhibited low deuteration for I_{ADP} and *W*, while $I_{Mg\text{-}dep}$ displayed more extensive HDX (Figure 3, second column). The bimodal appearance of the $I_{Mg\text{-}dep}$ spectrum reveals mixed EX1/EX2 behavior in this region.[42] The enhanced β241-249 deuteration of $I_{Mg\text{-}dep}$ reflects a lack of nucleotide-induced stabilization, keeping in mind that $I_{Mg\text{-}dep}$ has a greatly reduced nucleotide binding affinity.[53,75,76] Similarly, β246-253 displayed more extensive deuteration under $I_{Mg\text{-}dep}$ conditions than for I_{ADP}, but for this peptide a high deuteration level persisted also under *W* conditions (Figure 3, third column). Thus, for the catalytic site peptides highlighted in Figure 3 only the P-loop HDX behavior can be directly linked to rotational catalysis. The other two peptides β241-249 and β246-253 are subject to ligand (nucleotide) binding effects that obscure HDX features associated with catalytic turnover.[77]

The ^{379}DELSEED^{386} region of the β-lever transmits power strokes to γ.[5,14] Surprisingly, peptides of the β-lever region showed deuteration patterns that were almost identical under all conditions (β382-388, fourth column of Figure 3). Hence, the H-bonding network in the DELSEED region is largely insensitive to the occurrence of power strokes.

The γ C-terminal helix deserves particular attention (exemplified by γ260-275, last column of Figure 3). For the inactive states I_{ADP} and $I_{Mg\text{-}dep}$ this region showed moderate deuteration. In contrast, γ rotation under *W* conditions caused significantly enhanced HDX levels, indicating a marked destabilization of the γ C-terminal helix. The bimodal EX1/EX2 isotope distribution of γ260-275 signifies conformational dynamics on a wide range of time scales,[42] including H-bond

opening/closing transitions taking place much faster and much slower than $k_{int} \approx 10\ s^{-1}$. From the gradual intensity increase of the high mass component the EX1 opening rate constant can be estimated to be around $k_{op} \approx 0.01\ min^{-1}$. Other peptides in the γ C-terminal helix showed a behavior very similar to that discussed here for γ260-275 (Figure S3).

HDX Difference Plots. To visualize the behavior of all ~150 peptides we generated HDX difference plots for t = 45 min, with I_{ADP} as reference state (Figure S4). These plots were mapped to the F_1-ATPase crystal structure (Figure 4). Absolute HDX levels for I_{ADP} are shown in Figure 4a. Complete deuteration profiles for all peptides are summarized in the SI Appendix.

HDX differences of $I_{AMP\text{-}PNP}$ vs. I_{ADP} were close to zero across the entire protein complex, implying that the H-bond dynamics of the two forms are very similar (Figure 4b). $I_{Mg\text{-}dep}$ showed elevated HDX levels compared to I_{ADP} for several β segments, covering residues 150 to 280 which include the catalytic site (Figure 4c, e). As noted, these enhanced dynamics are attributed to the low nucleotide binding affinity of $I_{Mg\text{-}dep}$ which results in a lack of ligand-induced stabilization compared to I_{ADP}.[25,52,53]

Elevated deuteration around the β catalytic site was also evident for W (Figure 4d, f). This HDX enhancement was most pronounced around residue 300, i.e., the β catch loop that interacts with γ and coordinates nucleotide binding/release during γ rotation.[78] It is tempting to ascribe these enhanced β dynamics of W to catalytic motions. However, the occurrence of very similar dynamics enhancements for $I_{Mg\text{-}dep}$ implies that such an interpretation would be tenuous. A more cautionary view is that catalytic events (in W) and a lack of nucleotide-induced stabilization (in $I_{Mg\text{-}dep}$) both give rise to β fluctuations that cause enhanced deuteration.

The feature most clearly and uniquely linked to rotational catalysis was the elevated EX1/EX2 deuteration of the γ C-terminal helix under *W* conditions (arrows in Figure 4d, f). Thus, during γ rotation in F_1-ATPase H-bonds in the γ C-terminal helix get destabilized. We propose that this effect arises from interactions between the γ C-terminal helix and $\alpha_3\beta_3$. More specifically we envision that, while the β-levers force γ to turn, the γ C-terminal helix experiences rotational resistance in the apical bearing. This resistance causes helix over-twisting. Occasionally the rotor tip stalls and undergoes local unfolding, evident from the enhanced deuteration of the γ C-terminal helix (Figure 4d, f). The local unfolding events at the rotor tip are equivalent to the EX1 opening transitions noted previously (Figure 3 bottom right, Figure S3).

The aforementioned interpretation of HDX data in terms of rotational resistance ("friction") in F_1-ATPase is reminiscent of our previous work on F_oF_1.[40] However, one has to reconcile this proposed F_1-ATPase scenario with the fact that γ destabilization in F_oF_1 takes place only in the presence of PMF,[40] while for F_1-ATPase this phenomenon occurs without an energized membrane. From the following sections it will be seen that the surprising vulnerability of the γ C-terminal helix in F_1-ATPase reflects the absence of a membrane-anchored c_{10} ring that stabilizes the rotation axis in the case of intact F_oF_1. We will demonstrate that all of the available data support the proposed scenario, where $\gamma\cdots\alpha_3\beta_3$ contacts in the apical bearing of F_1-ATPase favor occasional stalling and unfolding of the apical rotor tip during catalytic turnover.

A Pertinent Side Aspect - The Role of ε. Under certain conditions the ε C-terminus can adopt an extended conformation that protrudes into $\alpha_3\beta_3$ and inhibits γ rotation.[10,12,13,79,80] In contrast, during rotational catalysis the ε C-terminus is folded towards the γ foot,[80] as seen in some thermophiles,[81] and for the mitochondrial "δ" homolog of ε.[7] Is it possible that the HDX properties

of the γ C-terminal helix tip arise from this conformational switching of ε? Several lines of evidence indicate that this is not the case. In the apical bearing γ is tightly surrounded by $\alpha_3\beta_3$ side chains,[80] and the region that gets destabilized under *W* conditions is not in direct contact with the ε C-terminus (Figures 1a, 4d). This spatial separation makes it unlikely that ε affects the behavior of γ within the apical bearing.[13] More importantly, the HDX properties of the ε C-terminus in $I_{Mg\text{-}dep}$ and $I_{AMP\text{-}PNP}$ are quite different, but the γ C-terminal helix remains protected under both conditions (Figure S4a, b). This behavior argues against strong conformational crosstalk between ε and the γ C-terminal helix tip. Instead, the elevated deuteration of γ C-terminal helix under *W* conditions must be directly attributed to rotation of γ.

Enforced Bulk Rotation Simulations. For complementing our HDX-MS data we conducted steered MD simulations[54-56] on F_1-ATPase. As in previous work, 120° rotation segments of γ were modeled within the $\alpha_3\beta_3\gamma$ complex.[17,20,21,48,56,67,73,74,82-86] Subunits δ and ε (which do not participate in F_1 power transmission) were omitted.[2,16] While allowing for some torsional elasticity of γ,[2] previously used MD protocols forced γ to maintain conformations relatively close to the crystal structure. In addition, previous work used restraints to keep the rotation axis close to the $\alpha_3\beta_3$ centerline.[17,56,67,73] Such heuristic restraints promote stable simulation runs, but they likely paint an overly restrictive picture of the conformational freedom experienced by γ.

For illustrative purposes we initially simulated the behavior of γ using enforced bulk rotation, which represents a well-established restrained protocol.[73,74] Under this scheme, γ experienced a global torque resulting from forces that were applied simultaneously to all γ residues (Figure 2a). By design, this algorithm caused the entire γ subunit to perform a 120° turn without

major deformation (Figure 5a-c). The γ C-terminal helix rotated with the rest of γ (Figure 5d) and without disruption of its H-bonding network (Figure 6a, b). The $\alpha_3\beta_3$ head smoothly accommodated rotation of γ by passively moving β levers, apical bearing side chains, and other segments (Supporting Movie 1). We do not dispute the usefulness of such enforced bulk rotation simulations for exploring certain aspects of $\alpha_3\beta_3\gamma$ operation.[21,67,73,74,86] However, this approach did not reproduce the HDX-detected destabilization of the γ C-terminal helix (Figure 4d, f).

Off-Axis Force Simulations. The MD strategy used in the preceding paragraph does not reflect the actual forces experienced by γ in F_1-ATPase. Under *in vitro* conditions, γ rotation is driven by β lever power strokes that apply *off-axis* forces to relatively few residues in the γ coiled coil.[16,17,56,87] Karplus[17] proposed an off-axis force method for modeling this type of torque generation. While Karplus' method[17] represented a major advance, it employed a stabilizing plastic network to minimize deformation of γ. Additional restraints were applied to eliminate tilting of the rotation axis.[17] As pointed out before, such restraints likely mask some of the conformational flexibility associated with rotational catalysis.

Here we devised an off-axis force method similar to that of Karplus,[17] except that deformation and tilting of γ were not suppressed by restraints. Rotation was driven by COM pulling[55] of γ20-26 which represents the key γ/β interaction region during power strokes.[56] Figure 5e-p displays data from three off-axis force runs. In each case, γ20-26 rotated along the expected 120° arc, together with parts of the γ coiled coil. The trajectories of other γ segments were less orderly and varied from run to run. The γ foot exhibited considerable lateral movement (exemplified by the orange trace of Figure 5f), implying that γ did not rotate on a stable axis. This

behavior reflects the interplay of COM pulling forces and reaction forces exerted by $\alpha_3\beta_3$, keeping in mind that F_1-ATPase lacks a c_{10} bearing that would stabilize rotation of γ (Figure 1).

Importantly, the end of the γ C-terminal helix did not rotate in any of the off-axis force simulations, i.e., it remained stuck (stalled) in the apical bearing (Figure 5g, k, o). At the conclusion of the 120° runs, the (non-rotating) end of the γ C-terminal helix was separated from the (rotating) lower part by a kink in the over-twisted helix (Figure 5h, l, p, Supporting Movie 2). These rotation-induced kinks caused H-bonds in the γ C-terminal helix to dissociate (Figure 6c-e).

Each of the three off-axis force runs triggered H-bond opening in slightly different positions close to the end of the γ C-terminal helix. Gratifyingly, all these opening events were located in the γ region that exhibited strongly enhanced HDX under *W* conditions (Figure 6c-e, Figure 4d, f). Thus, HDX experiments and MD simulations independently identified the same segment of the γ C-terminal helix as being destabilized during rotation. The MD simulations did not predict any other major H-bond disruption, consistent with the HDX data which did not indicate any other deuteration hot spots in γ (Figure 4d, f). Our MD data were further corroborated in simulations on *E. coli* and bovine F_1-ATPase using various nucleotide occupancies and rotation speeds, attesting to the robustness of our results (Figures S6, S7).

Behavior of the Apical Bearing. When considered in isolation, the interpretation of HDX data (Figure 4) may be open to debate. In contrast, our MD trajectories provide unequivocal insights into the reasons underlying the opening of H-bonds in the γ C-terminal helix. These H-bonds rupture because the apical end of the rotor tends to stall in the apical bearing, while power strokes force the rest of γ to rotate. These conditions give rise to over-twisting of the γ C-terminal helix, resulting in transient unfolding of the rotor shaft. The unfolding events take place where the γ

coiled coil transitions into a single helix, i.e., where the rotor is most fragile (Figure 5e, i, m). Taken together, our HDX experiments and MD simulations provide a consistent view of the destabilizing factors experienced by the γ C-terminal helix.

Previous work implied that the hydrophobic nature of the γ···$\alpha_3\beta_3$ interface in the apical bearing would provide a low friction environment that facilitates rotation of the γ C-terminal helix.[14] The current results imply that this classical "greasy bearing" model[14,57] has to be revised. Our MD data demonstrate that hydrophobic contacts and steric clashes of nonpolar side chains interfere with smooth rotation of the γ C-terminal helix. Examples of such contacts include γ(I272/L276/V280) with β(M261/P262/V265), illustrated in Figure S7. Side chain H-bonds and salt bridges dissociate more readily and do not impede rotation to the same extent (Figure S7).

What are the implications of our combined HDX/MD data for the mechanism of γ rotation in F_1-ATPase? At short HDX times (e.g., 10 s, Figure S2) the γ C-terminal helix under *W* conditions only shows a minor (< 1%) high mass EX1 component. This finding demonstrates that the steady-state population of F_1-ATPase molecules with an intact γ C-terminal helix is on the order of 99%. In other words, at any instant only a fraction of the catalytically active (*W*) F_1-ATPase complexes possess a disrupted γ rotor. The EX1 nature of the γ HDX kinetics implies that the catalytically active complexes only occasionally transition into the unfolded γ conformation (with $k_{op} \approx 0.01$ min^{-1}). They remain in this state for time periods longer than k_{int}^{-1} (≈ 0.1 s), and then switch back to the intact rotor structure.[32,42-44] It is possible that these refolding events take place after γ has completed a 360° rotation, such that the residues of the disrupted rotor tip are once again pre-aligned to assemble into an intact γ C-terminal helix.

Critics might argue that the HDX-detected *occasional* unfolding of γ differs from the MD simulations where *each* power stroke resulted in opening of the γ C-terminal helix. We attribute

this discrepancy to the different rotation rates, *i.e.*, ~3° ns^{-1} in the MD runs vs. ~3×10^{-4} ° ns^{-1} under experimental conditions.[16] The slower rotation in the experiments provides more time for clashing side chains in the apical bearing to sample conformations that facilitate rotational gliding of the torsionally strained helix during power strokes.[20] Phenomenologically, this gliding will resemble the behavior seen in enforced rotation runs (Figure 6a-d / Figure S7a). It would be desirable to confirm this time dependence by conducting off-axis force MD runs at much lower rotation rates, but unfortunately such endeavors are not feasible due to their enormous computational cost. As noted, the rotation rates employed here are within the range used for previous investigations.[17,20,56,67,73,74] Despite the difference in time scale, it is remarkable how well the MD-predicted H-bond opening events agree with the experimentally detected HDX hot spot in the γ C-terminal helix (Figure 6c-e).

Conclusions

Steered MD protocols and related modeling approaches have previously been applied to ATPases,[17,20,21,48,56,67,73,74,82-86,88] but none of those studies focused on the γ C-terminal helix and apical bearing. The MD strategy devised here explicitly considered the off-axis nature of power strokes, while avoiding heuristic conformational/orientational restraints. In this way, key properties of the γ rotor could be uncovered. Specifically, we were able to provide the mechanistic basis of the experimentally observed H-bond destabilization in the γ C-terminal helix. We found that the torsionally strained γ C-terminal helix is predisposed to stall and unfold, as governed by the interplay of resistive forces in the apical bearing and β-lever power strokes. We envision that

once F_1-ATPase is in this locally unfolded state, rotation of γ continues via swivel motions around ϕ/Ψ dihedrals in the kinked segments, analogous to the crosslinked constructs of Hilbers et al.[51]

Interestingly, rotation of γ can take place even in F_1 constructs that have a severely truncated γ C-terminal helix (although those conditions result in reduced torque).[89,90] Thus, rotational catalysis is compatible with various scenarios in the apical bearing; these include conditions where the rotor tip is absent,[89,90] immobilized by crosslinking,[51] or transiently unfolded (as seen in this work for wild-type F_1-ATPase).

In a previous HDX-MS investigation[40] we observed destabilization of the γ C-terminal helix in catalytically active F_oF_1, and we also attributed that effect to rotational resistance associated with γ···$\alpha_3\beta_3$ contacts in the apical bearing. Interestingly, in F_oF_1 this destabilization of γ was observed only during operation against a PMF-induced countertorque. The question arises why γ destabilization likewise takes place in F_1-ATPase which does not possess an energized membrane and lacks a PMF-induced countertorque. In addition to its apical bearing, the γ rotor in F_oF_1 is secured at its base by the membrane-bound c_{10} ring. Having a bearing at both ends will stabilize the rotation axis of γ (Figure 1a). In contrast, F_1-ATPase only possesses a single rotor bearing at the apical end of γ, while the γ foot is unsupported and protrudes into the solvent (Figure 1b). The lack of a basal (c_{10}) bearing results in an unstable rotation axis, with bending and lateral movements of γ during power strokes, as seen in Figure 5f. Such bending promotes the formation of helix kinks which trigger the disruption of H-bonds (Figure 5h, l, p).

This study marks the first time that HDX-MS and steered MD simulations were applied as complementary tools for deciphering the inner workings of a molecular machine, taking advantage of structural insights from X-ray crystallography and cryo-EM. Through further refinement of this

combined approach it should be possible to uncover additional details related to rotor operation, power transmission, and mechanochemical energy coupling.

Acknowledgement. We thank Yumin Bi for preparation of F_1-ATPase samples, and Vlad Popa for initial assistance with the computational aspects of this work.

Supporting Information. Additional Figures as indicated in the text. This material is available free of charge at http://pubs.acs.org.

References

(1) Walker, J. E. *Biochem. Soc. Trans.* **2013**, *41*, 1-16.
(2) Junge, W.; Nelson, N. *Annu. Rev. Biochem.* **2015**, *84*, 631-657.
(3) Borsch, M.; Duncan, T. M. *Biochem. Soc. Trans.* **2013**, *41*, 1219-1226.
(4) Mitchell, P. *Biochim. Biophys. Acta-Bioenerg.* **2011**, *1807*, 1507-1538.
(5) Sielaff, H.; Borsch, M. *Philos. Trans. R. Soc. B-Biol. Sci.* **2013**, *368*, 1-12.
(6) Wachter, A.; Bi, Y. M.; Dunn, S. D.; Cain, B. D.; Sielaff, H.; Wintermann, F.; Engelbrecht, S.; Junge, W. *Proc. Natl. Acad. Sci. U.S.A.* **2011**, *108*, 3924-3929.
(7) Hahn, A.; Parey, K.; Bublitz, M.; Mills, D. J.; Zickermann, V.; Vonck, J.; Kuhlbrandt, W.; Meier, T. *Mol. Cell* **2016**, *63*, 445-456.
(8) Mazhab-Jafari, M. T.; Rohou, A.; Schmidt, C.; Bueler, S. A.; Benlekbir, S.; Robinson, C. V.; Rubinstein, J. L. *Nature* **2016**, *539*, 118-+.
(9) Zhou, A. N.; Rohou, A.; Schep, D. G.; Bason, J. V.; Montgomery, M. G.; Walker, J. E.; Grigorieff, N.; Rubinstein, J. L. *eLife* **2015**, *4*.
(10) Shirakihara, Y.; Shiratori, A.; Tanikawa, H.; Nakasako, M.; Yoshida, M.; Suzuki, T. *FEBS J.* **2015**, *282*, 2895-2913.
(11) Morales-Rios, E.; Montgomery, M. G.; Leslie, A. G. W.; Walker, J. E. *Proc. Natl. Acad. Sci. U.S.A.* **2015**, *112*, 13231-13236.
(12) Sobti, M.; Smits, C.; Wong, A. S. W.; Ishmukhametov, R.; Stock, D.; Sandin, S.; Stewart, A. G. *eLife* **2016**, *5*.
(13) Cingolani, G.; Duncan, T. M. *Nat. Struct. Mol. Biol.* **2011**, *18*, 701-708.
(14) Abrahams, J. P.; Leslie, A. G. W.; Lutter, R.; Walker, J. E. *Nature* **1994**, *370*, 621-628.
(15) Mnatsakanyan, N.; Krishnakumar, A. M.; Suzuki, T.; Weber, J. *J. Biol. Chem.* **2009**, *284*, 11336-11345.
(16) Martin, J. L.; Ishmukhametov, R.; Hornung, T.; Ahmad, Z.; Frasch, W. D. *Proc. Natl. Acad. Sci. U.S.A.* **2014**, *111*, 3715-3720.
(17) Nam, K.; Pu, J. Z.; Karplus, M. *Proc. Natl. Acad. Sci. U.S.A.* **2014**, *111*, 17851-17856.
(18) Ishmukhametov, R.; Hornung, T.; Spetzler, D.; Frasch, W. D. *EMBO J.* **2010**, *29*, 3911-3923.
(19) Symersky, J.; Pagadala, V.; Osowski, D.; Krah, A.; Meier, T.; Faraldo-Gomez, J. D.; Mueller, D. M. *Nat. Struct. Mol. Biol.* **2012**, *19*, 485-491.
(20) Okazaki, K.; Hummer, G. *Proc. Natl. Acad. Sci. U.S.A.* **2015**, *112*, 10720-10725.
(21) Czub, J.; Wieczor, M.; Prokopowicz, B.; Grubmuller, H. *J. Am. Chem. Soc.* **2017**, *139*, 4025-4034.
(22) Uchihashi, T.; Iino, R.; Ando, T.; Noji, H. *Science* **2011**, *333*, 755-758.
(23) Noji, H.; Yasuda, R.; Yoshida, M.; Kinosita, K. *Nature* **1997**, *386*, 299-302.
(24) Yasuda, R.; Noji, H.; Kinosita, K.; Yoshida, M. *Cell* **1998**, *93*, 1117-1124.
(25) Hirono-Hara, Y.; Noji, H.; Nishiura, M.; Muneyuki, E.; Hara, K. Y.; Yasuda, R.; Kinosita, K.; Yoshida, M. *Proc. Natl. Acad. Sci. U.S.A.* **2001**, *98*, 13649-13654.
(26) Adachi, K.; Yasuda, R.; Noji, H.; Itoh, H.; Harada, Y.; Yoshida, M.; Kinosita, K. *Proc. Natl. Acad. Sci. U. S. A.* **2000**, *97*, 7243-7247.
(27) Kato-Yamada, Y.; Noji, H.; Yasuda, R.; Kinosita, K.; Yoshida, M. *J. Biol. Chem.* **1998**, *273*, 19375-19377.
(28) Pirrone, G. F.; Iacob, R. E.; Engen, J. R. *Anal. Chem.* **2015**, *87*, 99-118.
(29) Rand, K. D.; Zehl, M.; Jorgensen, T. J. D. *Acc. Chem. Res.* **2014**, *47*, 3018-3027.
(30) Kaltashov, I. A.; Bobst, C. E.; Abzalimov, R. R. *Protein Sci.* **2013**, *22*, 530-544.

(31) Chalmers, M. J.; Busby, S. A.; Pascal, B. D.; West, G. M.; Griffin, P. R. *Exp. Rev. Proteomics* **2011**, *8*, 43-59.
(32) Percy, A. J.; Rey, M.; Burns, K. M.; Schriemer, D. C. *Anal. Chim. Acta* **2012**, *721*, 7-21.
(33) Malhotra, P.; Udgaonkar, J. B. *J. Am. Chem. Soc.* **2016**, *138*, 5866-5878.
(34) Zhang, Y.; Rempel, D. L.; Zhang, J.; Sharma, A. K.; Mirica, L. M.; Gross, M. L. *Proc. Natl. Acad. Sci. U.S.A.* **2013**, *110*, 14604-14609.
(35) Lee, S.; Wales, T. E.; Escudero, S.; Cohen, D. T.; Luccarelli, J.; Gallagher, C. G.; Cohen, N. A.; Huhn, A. J.; Bird, G. H.; Engen, J. R.; Walensky, L. D. *Nat. Struct. Mol. Biol.* **2016**, *23*, 600-607.
(36) Huang, R. Y. C.; Chen, G. D. *Anal. Bioanal. Chem.* **2014**, *406*, 6541-6558.
(37) Hvidt, A.; Nielsen, S. O. *Adv. Protein Chem.* **1966**, *21*, 287-386.
(38) Englander, S. W.; Mayne, L.; Krishna, M. M. G. *Quart. Rev. Biophys.* **2007**, *40*, 287-326.
(39) Cipriano, D. J.; Dunn, S. D. *J. Biol. Chem.* **2002**, *277*, 16782–16790.
(40) Vahidi, S.; Bi, Y. M.; Dunn, S. D.; Konermann, L. *Proc. Natl. Acad. Sci. U.S.A.* **2016**, *113*, 2412-2417.
(41) Bai, Y.; Milne, J. S.; Mayne, L.; Englander, S. W. *Proteins: Struct., Funct., Genet.* **1993**, *17*, 75-86.
(42) Xiao, H.; Hoerner, J. K.; Eyles, S. J.; Dobo, A.; Voigtman, E.; Mel'Cuk, A. I.; Kaltashov, I. A. *Protein Sci.* **2005**, *14*, 543-557.
(43) Konermann, L.; Tong, X.; Pan, Y. *J. Mass Spectrom.* **2008**, *43*, 1021-1036.
(44) Weis, D. D.; Wales, T. E.; Engen, J. R.; Hotchko, M.; Ten Eyck, L. F. *J. Am. Soc. Mass Spectrom.* **2006**, *17*, 1498-1509.
(45) Kapulainen, M.; Ronkainen, H.; Hokkanen, A.; Stuns, I.; Varjus, S.; Nyyssonen, S.; Turunen, R.; Halme, J. *Tribol. Lett.* **2014**, *56*, 47-54.
(46) Ueno, H.; Suzuki, T.; Kinosita, K.; Yoshida, M. *Proc. Natl. Acad. Sci. U.S.A.* **2005**, *102*, 1333-1338.
(47) Adachi, K.; Oiwa, K.; Nishizaka, T.; Furuike, S.; Noji, H.; Itoh, H.; Yoshida, M.; Kinosita, K. *Cell* **2007**, *130*, 309-321.
(48) Mukherjee, S.; Bora, R. P.; Warshel, A. *Q. Rev. Biophys.* **2015**, *48*, 395-403.
(49) Ito, Y.; Ikeguchi, M. *Biophys. J.* **2015**, *108*, 85-97.
(50) Bason, J. V.; Montgomery, M. G.; Leslie, A. G. W.; Walker, J. E. *Proc. Natl. Acad. Sci. U. S. A.* **2015**, *112*, 6009-6014.
(51) Hilbers, F.; Junge, W.; Sielaff, H. *PLOS One* **2013**, *8*.
(52) Bowler, M. W.; Montgomery, M. G.; Leslie, A. G. W.; Walker, J. E. *Proc. Natl. Acad. Sci. U.S.A.* **2006**, *103*, 8646-8649.
(53) Weber, J.; Wilkemounts, S.; Senior, A. E. *J. Biol. Chem.* **1994**, *269*, 20462-20467.
(54) Isralewitz, B.; Gao, M.; Schulten, K. *Curr. Opin. Struct. Biol.* **2001**, *11*, 224-230.
(55) Lemkul, J. A.; Bevan, D. R. *J. Phys. Chem. B* **2010**, *114*, 1652-1660.
(56) Pu, J.; Karplus, M. *Proc. Natl. Acad. Sci. U.S.A.* **2008**, *105*, 1192-1197.
(57) Sokolov, M.; Lu, L.; Tucker, W.; Gao, F.; Gegenheimer, P. A.; Richter, M. L. *J. Biol. Chem.* **1999**, *274*, 13824-13829.
(58) Downie, J. A.; Langman, L.; Cox, G. B.; Yanofsky, C.; Gibson, F. *J. Bacteriol.* **1980**, *143*, 8-17.
(59) Dunn, S. D.; Tozer, R. G.; Antczak, D. F.; Heppel, L. A. *J. Biol. Chem.* **1985**, *260*, 418-425.
(60) Glasoe, P. K.; Long, F. A. *J. Phys. Chem.* **1960**, *64*, 188-190.
(61) Kaltashov, I. A.; Bobst, C. E.; Abzalimov, R. R. *Anal. Chem.* **2009**, *81*, 7892-7899.
(62) Smith, D. L.; Deng, Y.; Zhang, Z. *J. Mass Spectrom.* **1997**, *32*, 135-146.

(63) Abraham, M. J.; Murtola, T.; Schulz, R.; Páll, S.; Smith, J. C.; Hess, B.; Lindahl, E. *SoftwareX* **2015**, *1–2*, 19-25.
(64) Huang, J.; MacKerell, A. D. *J. Comput. Chem.* **2013**, *34*, 2135-2145.
(65) Jorgensen, W. L.; Chandrasekhar, J.; Madura, J. D.; Impey, R. W.; Klein, M. L. *J. Chem. Phys.* **1983**, *79*, 926-935.
(66) Gibbons, C.; Montgomery, M. G.; Leslie, A. G. W.; Walker, J. E. *Nat. Struct. Biol.* **2000**, *7*, 1055-1061.
(67) Okazaki, K.; Hummer, G. *Proc. Natl. Acad. Sci. U.S.A.* **2013**, *110*, 16468-16473.
(68) Essmann, U.; Perera, L.; Berkowitz, M. L.; Darden, T.; Lee, H.; Pedersen, L. G. *J. Chem. Phys.* **1995**, *103*, 8577-8593.
(69) Bussi, G.; Donadio, D.; Parrinello, M. *J. Chem. Phys.* **2007**, *126*, 0141011-0141017.
(70) Parrinello, M.; Rahman, A. *J. Appl. Phys.* **1981**, *52*, 7182-7190.
(71) Hoover, W. G. *Phys. Rev. A* **1985**, *31*, 1695-1697.
(72) Hess, B.; Kutzner, C.; van der Spoel, D.; Lindahl, E. *J. Chem. Theory Comput.* **2008**, *4*, 435-447.
(73) Kutzner, C.; Czub, J.; Grubmuller, H. *J. Chem. Theory Comput.* **2011**, *7*, 1381-1393.
(74) Czub, J.; Grubmuller, H. *J. Am. Chem. Soc.* **2014**, *136*, 6960-6968.
(75) Zhu, M. M.; Rempel, D. L.; Du, Z. H.; Gross, M. L. *J. Am. Chem. Soc.* **2003**, *125*, 5252-5253.
(76) Ghaemmaghami, S.; Fitzgerald, M. C.; Oas, T. G. *Proc. Natl. Acad. Sci. U.S.A.* **2000**, *97*, 8296-8301.
(77) Fast, C. S.; Vahidi, S.; Konermann, L. *Anal. Chem.* **2017**, *89*, 13326-13333.
(78) Greene, M. D.; Frasch, W. D. *J. Biol. Chem.* **2003**, *278*, 51594-51598.
(79) Dallmann, H. G.; Flynn, T. G.; Dunn, S. D. *J. Biol. Chem.* **1992**, *267*, 18953-18960.
(80) Shah, N. B.; Hutcheon, M. L.; Haarer, B. K.; Duncan, T. M. *J. Biol. Chem.* **2013**, *288*, 9383-9395.
(81) Ferguson, S. A.; Cook, G. M.; Montgomery, M. G.; Leslie, A. G. W.; Walker, J. E. *Proc. Natl. Acad. Sci. U. S. A.* **2016**, *113*, 10860-10865.
(82) Dittrich, M.; Hayashi, S.; Schulten, K. *Biophys. J.* **2004**, *87*, 2954-2967.
(83) Mukherjee, S.; Warshel, A. *Proc. Natl. Acad. Sci. U.S.A.* **2011**, *108*, 20550-20555.
(84) Mukherjee, S.; Warshel, A. *Proc. Natl. Acad. Sci. U.S.A.* **2015**, *112*, 2746-2751.
(85) Koga, N.; Takada, S. *Proc. Natl. Acad. Sci. U.S.A.* **2006**, *103*, 5367-5372.
(86) Czub, J.; Grubmuller, H. *Proc. Natl. Acad. Sci. U.S.A.* **2011**, *108*, 7408-7413.
(87) Junge, W.; Sielaff, H.; Engelbrecht, S. *Nature* **2009**, *459*, 364-370.
(88) Isaka, Y.; Ekimoto, T.; Kokabu, Y.; Yamato, I.; Murata, T.; Ikeguchi, M. *Biophys. J.* **2017**, *112*, 911-920.
(89) Hossain, M. D.; Furuike, S.; Maki, Y.; Adachi, K.; Suzuki, T.; Kohori, A.; Itoh, H.; Yoshida, M.; Kinosita, K. *Biophys. J.* **2008**, *95*, 4837-4844.
(90) Furuike, S.; Hossain, M. D.; Maki, Y.; Adachi, K.; Suzuki, T.; Kohori, A.; Itoh, H.; Yoshida, M.; Kinosita, K. *Science* **2008**, *319*, 955-958.
(91) Torshin, I. Y.; Weber, I. T.; Harrison, R. W. *Protein Eng.* **2002**, *15*, 359-363.

Figure Captions

Figure 1. (a) *E. coli* F_oF_1 architecture based on pdb file 3OAA.[12,13] One αβ pair facing the observer has been omitted to expose the γ rotor (termini of the γ are denoted as γN and γC). Catalytic site and β-lever are highlighted for one of the three β subunits. (b) F_1-ATPase. The figure highlights the apical bearing, where the γ C-terminal helix is seated within the $\alpha_3\beta_3$ head.

Figure 2. Schematic depiction of two different steered MD strategies used to drive a 120° rotation of γ in F_1-ATPase. (a) Enforced bulk rotation, where forces are applied to all residues of γ. (b) Off-axis force rotation, where forces are applied only to γ20-26 (green), mimicking the action of β-lever power strokes. The blue circle in (b) indicates the γ20-26 trajectory. All simulations were performed on the $\alpha_3\beta_3\gamma$ complex; two α and two β chains are not shown to reduce clutter. The β subunit depicted here is β_{empty}, which is poised to bind ATP and initiate the power stroke.

Figure 3. HDX mass spectra of selected F_1-ATPase peptides at t = 45 min under three conditions: I_{ADP} (top row), I_{Mg_dep} (middle row), and W (bottom row). The identity of each peptide is indicated along the top. Red dotted lines indicate centroid m/z values. Some of the spectra reveal EX1 behavior. For I_{ADP} and I_{Mg_dep} the P-loop peptide β148-159 data can be deconvoluted into three Gaussians with equal areas, consistent with three non-interconverting conformations β_{ATP}, β_{ADP}, and β_{empty}. During rotational catalysis (W) this spectrum coalesces into a single band.

Figure 4. HDX patterns for t = 45 min mapped to the F_1-ATPase crystal structure 3OAA.[13] (a) Absolute HDX levels for I_{ADP}. The β catch loop is highlighted by an asterisk. All other panels

represent HDX difference maps. Red indicates elevated deuteration, blue signifies less deuteration relative to I_{ADP}. (b) Difference map for $I_{AMP\text{-}PNP}$. (c) Difference map for $I_{Mg\text{-}dep}$. (d) Difference map for *W*. (e) Close-up view of the β catalytic site in $I_{Mg\text{-}dep}$ (f) Close-up view of the β catalytic site in *W*. Red arrows in (d), (f) highlight the region where the γ C-terminal helix gets destabilized during rotation under *W* conditions.

Figure 5. MD results for *E. coli* F_1-ATPase. 120° simulation were conducted on $\alpha_3\beta_3\gamma$. Not all subunits are shown to reduce clutter. (a-d) Enforced bulk rotation of γ. (e-p) γ Rotation by off-axis force simulations: run 1 at 3.9˚ ns^{-1}, run 2 at 3.3˚ ns^{-1}, run 3 at 4.8˚ ns^{-1}. *Top row:* final (120°) structures; *Second row:* y/z trajectories of γ segments: γ277 at the top of the γ C-terminal helix (cyan), γ58 at the base of γ (orange), and γ20-26 (green, pulling group for off-axis force rotation). Blue circles indicate expected γ20-26 trajectories. *Third row:* initial (magenta) and final (gray) γ conformations and orientations. *Bottom row:* C-terminal segment γ236-284 at the end of the MD runs. Arrows indicate MD-predicted H-bond opening during off-axis force rotation. The segments above these arrows were stalled ("stuck") and did not participate in γ rotation. Red color in the two bottom rows highlights regions that showed enhanced HDX during rotation (cf. Figures 4d, f).

Figure 6. Backbone NH···OC distances in γ from MD simulations. Values > 0.25 nm (dashed horizontal line)[91] represent disrupted H-bonds. Only NH sites that are H-bonded in the crystal structure are included. (a) Equilibrated structure prior to rotation. (b) After 120° enforced bulk rotation. (c) After 120° off-axis force rotation, run 1 at 3.9˚ ns^{-1}. (d) Ditto, run 2 at 3.3˚ ns^{-1}. (e) Ditto, run 3 at 4.8˚ ns^{-1}. Arrows highlight H-bond opening predicted in off-axis force simulations. Red indicates regions of enhanced deuteration in HDX experiments (cf. Figures 4d, f).

Figure 1

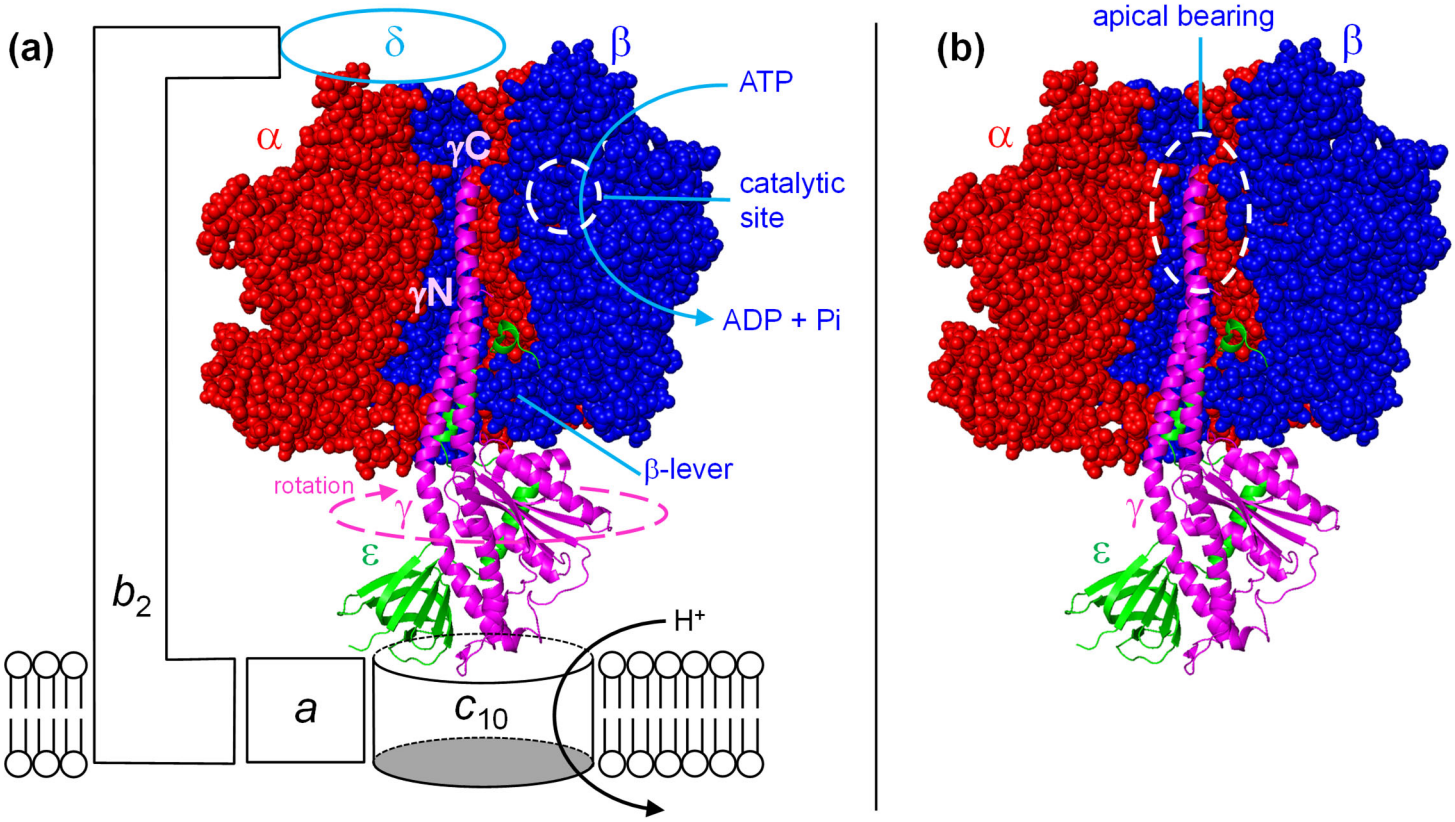
(a)
δ
β
α
γC
γN
ATP
catalytic site
ADP + Pi
β-lever
rotation
γ
ε
b2
a
c10
H+
(b)
apical bearing
β
α
γ
ε

Figure 2

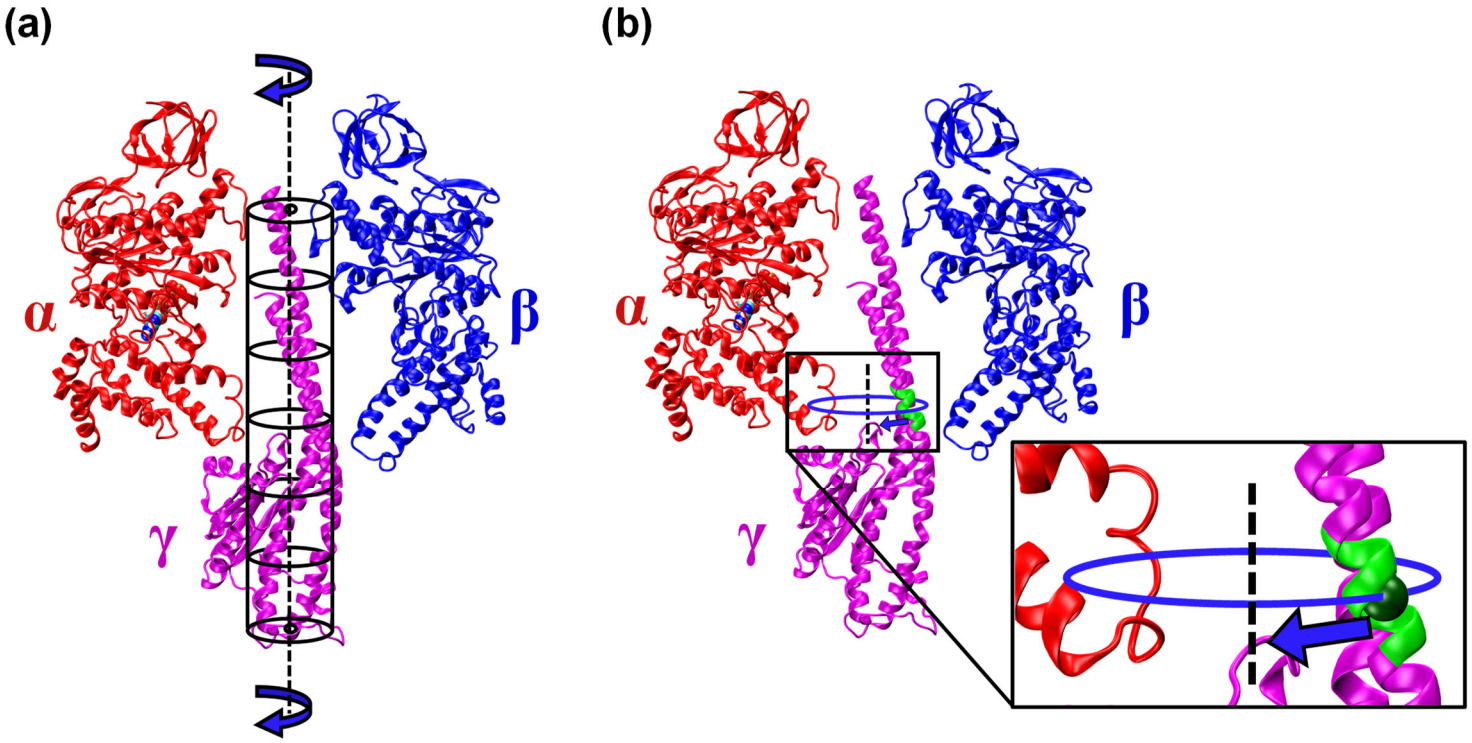

Figure 3

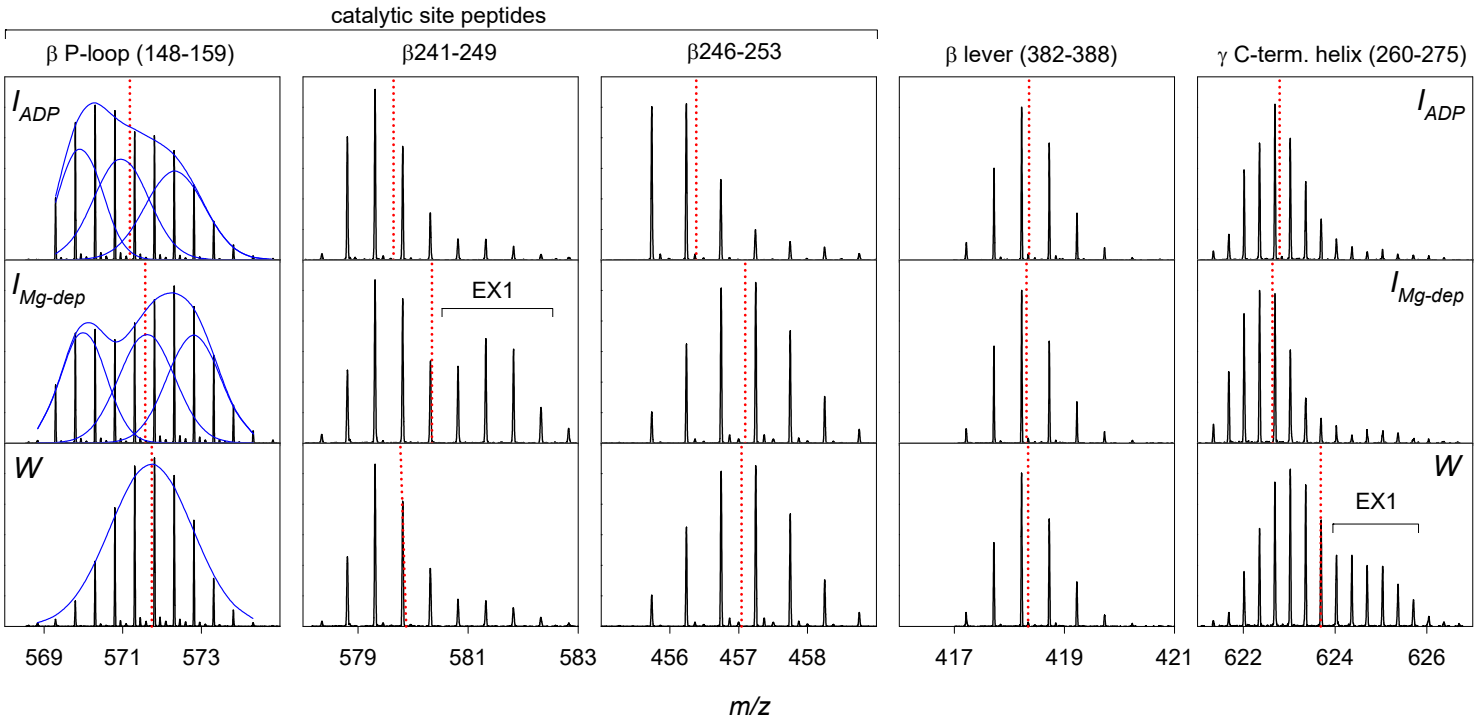
catalytic site peptides
β P-loop (148-159)
β241-249
β246-253
β lever (382-388)
γ C-term. helix (260-275)
I_{ADP}
$I_{Mg\text{-}dep}$
W
EX1
569
571
573
579
581
583
456
457
458
417
419
421
622
624
626
m/z

Figure 4

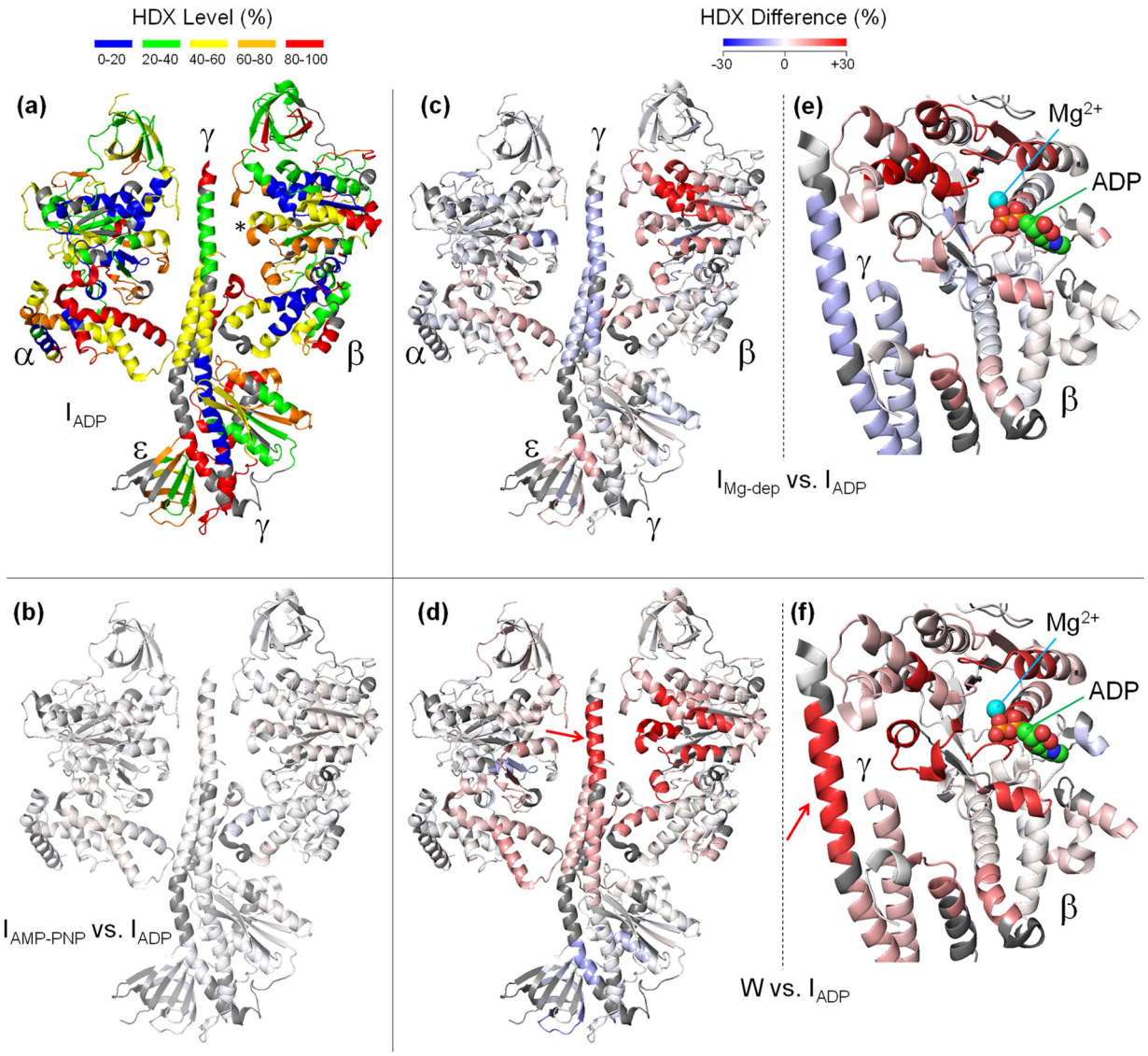
HDX Level (%)
0-20
20-40
40-60
60-80
80-100
HDX Difference (%)
-30
0
+30
(a)
(b)
(c)
(d)
(e)
(f)
γ
α
β
ε
*
I_ADP
I_AMP-PNP vs. I_ADP
I_Mg-dep vs. I_ADP
W vs. I_ADP
Mg2+
ADP

Figure 5

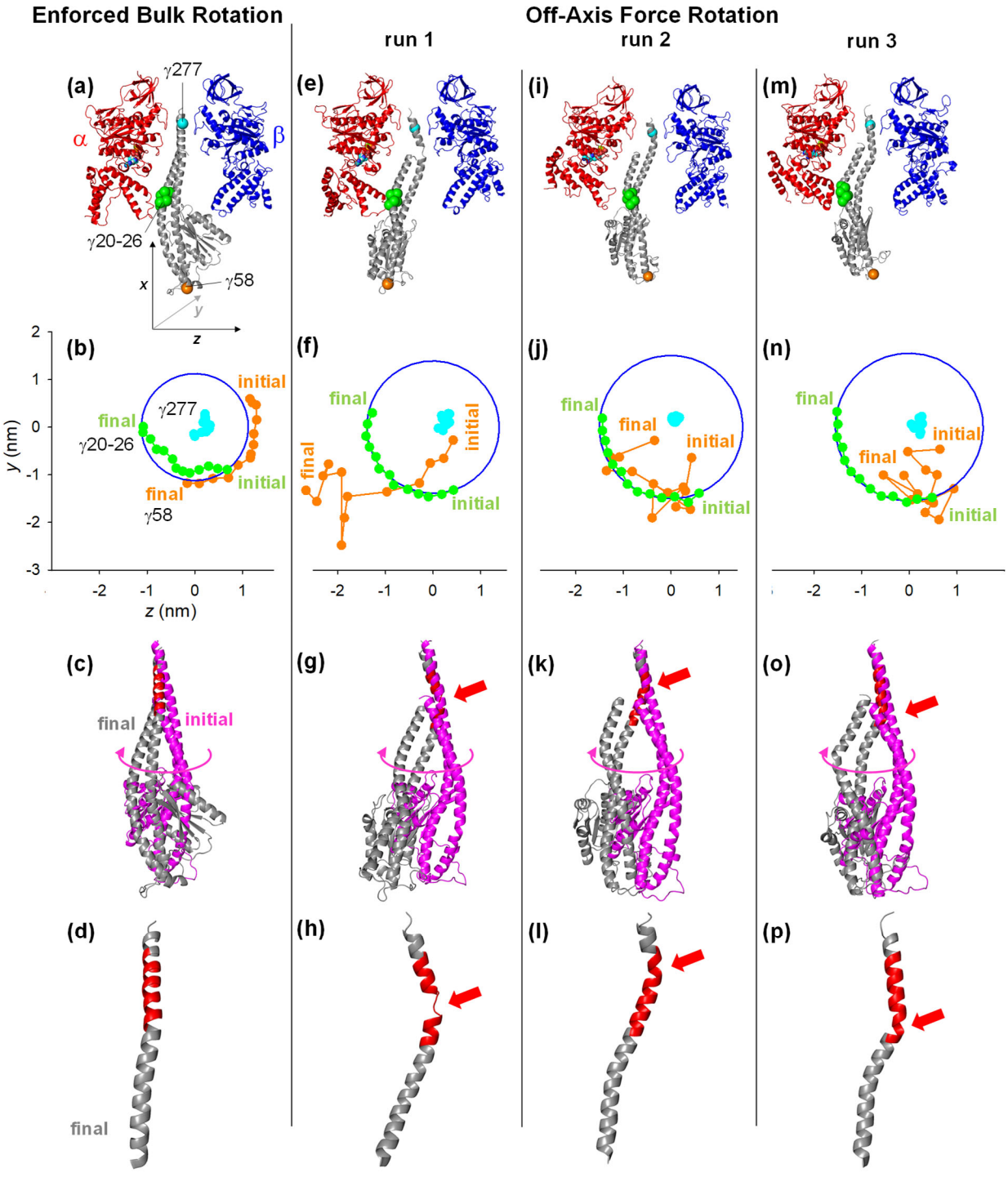
Enforced Bulk Rotation
Off-Axis Force Rotation
run 1
run 2
run 3
(a)
(b)
(c)
(d)
(e)
(f)
(g)
(h)
(i)
(j)
(k)
(l)
(m)
(n)
(o)
(p)
γ277
α
β
γ20-26
γ58
x
y
z
initial
final
y (nm)
z (nm)

Figure 6

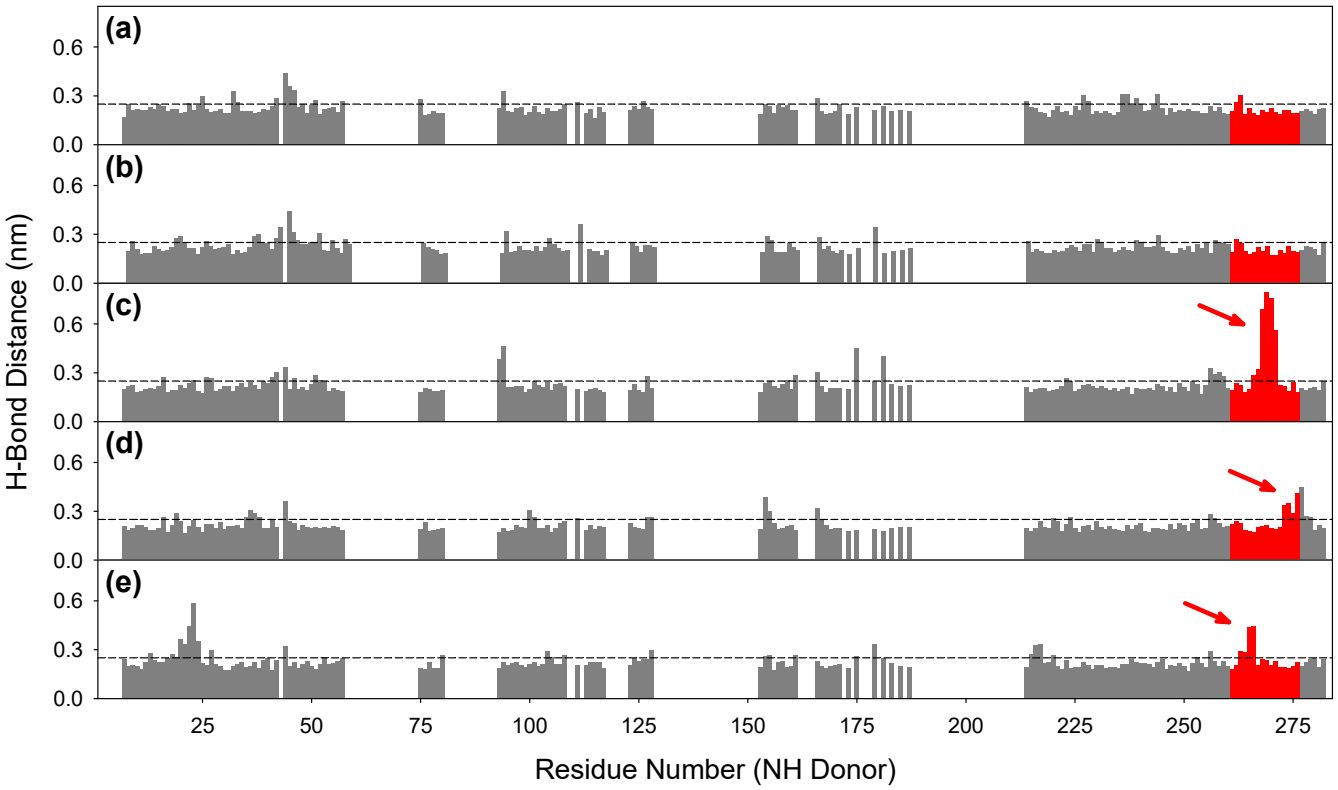
(a)
(b)
(c)
(d)
(e)
0.6
0.3
0.0
H-Bond Distance (nm)
25
50
75
100
125
150
175
200
225
250
275
Residue Number (NH Donor)

For Table of Contents Only